Title
Injection, flow, and mixing of CO2 in porous media with residual gas.

Authors
Oldenburg, C.M.
Doughty, C.A.

Publication Date
2010-12-01

Injection, Flow, and Mixing of CO_2 in Porous Media with Residual Gas

C.M. Oldenburg and Christine Doughty
Earth Sciences Division 90-1116
Lawrence Berkeley National Laboratory
Berkeley, CA USA
e-mail: cmoldenburg@lbl.gov
cadoughty@lbl.gov

Abstract

Geologic structures associated with depleted natural gas reservoirs are desirable targets for geologic carbon sequestration (GCS) as evidenced by numerous pilot and industrial-scale GCS projects in these environments world-wide. One feature of these GCS targets that may affect injection is the presence of residual CH_4. It is well known that CH_4 drastically alters supercritical CO_2 density and viscosity. Furthermore, residual gas of any kind affects the relative permeability of the liquid and gas phases, with relative permeability of the gas phase strongly dependent on the time-history of imbibition or drainage, i.e., dependent on hysteretic relative permeability. In this study, the effects of residual CH_4 on supercritical CO_2 injection were investigated by numerical simulation in an idealized one-dimensional system under three scenarios: (1) with no residual gas; (2) with residual supercritical CO_2; and (3) with residual CH_4. We further compare results of simulations that use non-hysteretic and hysteretic relative permeability functions. The primary effect of residual gas is to decrease injectivity by decreasing liquid-phase relative permeability. Secondary effects arise from injected gas effectively incorporating residual gas and thereby extending the mobile-gas plume relative to cases with no residual gas. Third-order effects arise from gas mixing and associated compositional effects on density that effectively create a larger plume per unit mass. Non-hysteretic models of relative permeability can be used to approximate some parts of the behavior of the system, but fully hysteretic formulations are needed to accurately model the entire system.

Introduction

Several geologic carbon sequestration (GCS) projects around the world involve CO_2 injection into depleted gas reservoirs. In some cases, injection is directly into the depleted reservoir (e.g., K12-B, van der Meer et al., 2007), while in others it is into the water leg of the reservoir (e.g., Otway Basin Pilot Project (Sharma et al., 2007); In Salah (Ringrose et al., 2009)). Regardless of the details of individual projects, injection into depleted reservoirs may involve injection into porous media that are filled predominantly with brine and residual methane (CH_4) gas.

There are numerous potential effects of residual CH_4 gas on supercritical CO_2 injection. First, residual gas of any kind will decrease the mobility of the brine, all other things being equal. Second, residual CH_4 provides an initial gas-phase saturation that can be mobilized and incorporated into the

injected plume, thereby increasing its size. Third, the mixing of CH_4 into supercritical CO_2 causes a large decrease in gas mixture density and viscosity that can affect the injectivity and mobility of the gas. In this study, the effects of residual gas on injection of supercritical CO_2 are investigated through modeling of an idealized one-dimensional radial system using TOUGH2/EOS7C (Oldenburg et al., 2004a) enhanced with hysteretic capillary pressure and relative permeabilty curves (Doughty, 2007). To evaluate and compare results, we refer to the concept of injectivity, defined loosely here as the pressure rise at the well for a given mass injection rate.

Motivation

Prior Work

There are numerous papers on the concept and evaluation of general feasibility of CO_2 injection into natural gas reservoirs for GCS and for enhanced gas recovery (Blok et al., 1992; Koide et al., 1992; van der Burght, 1992; Oldenburg et al., 2001; Oldenburg et al., 2004). In addition, studies of thermal effects of injecting high-pressure CO_2 into low-pressure depleted reservoirs have been made (Oldenburg, 2007; Maloney and Briceno, 2009; Mathias et al., 2010). The drastic changes in CO_2 properties arising from mixing with CH_4 are well known (e.g., Oldenburg et al., 2004b) and the associated potential beneficial uses have been noted (Oldenburg, 2007). None of these prior studies has investigated the effects of residual gas saturation in general, or the compositional effects associated with mixing supercritical CO_2 and residual CH_4 gas in particular. Furthermore, studies that compare hysteretic and non-hysteretic capillary pressure and relative permeability curves have focused on saline formations and CO_2 trapping (Doughty, 2007) rather than on depleted gas-reservoirs and CO_2 injectivity.

Effect of Residual Gas on Injection

Residual gas may affect an injection process in many different ways, e.g., inhibiting the displacement of brine through reduced relative permeability of brine, enhancing injection of gas as residual gas becomes mobile at the leading edge of the injected gas plume, or changing the composition of the gas and therefore gas-phase properties as injected gas mixes with residual gas of different composition. The purpose of this study is to investigate the processes of interaction between injected supercritical CO_2 and residual gas to understand potential implications for gas-reservoir injection projects in general. A simplified one-dimensional radial geometry is used to focus on mobility and gas composition effects. The idealized system was chosen to have a constant-pressure boundary condition at a radius of approximately 1 km to model injection into the water leg of a depleted gas-reservoir system with a nearby gas cap that would tend to moderate pressure rise due to injection.

Three different situations are shown in Figure 1 to illustrate the question being addressed. The base case is the injection of CO_2 into a system with no residual gas (Figure 1a). Figure 1b shows the case of injection of supercritical CO_2 into an aquifer with supercritical CO_2 at residual saturation. Lastly, Figure 1c shows the case of injection of supercritical CO_2 into a system with CH_4 at residual saturation. The specific question being addressed in this study is: what is the effect of residual gas and its composition on the injection of supercritical CO_2?

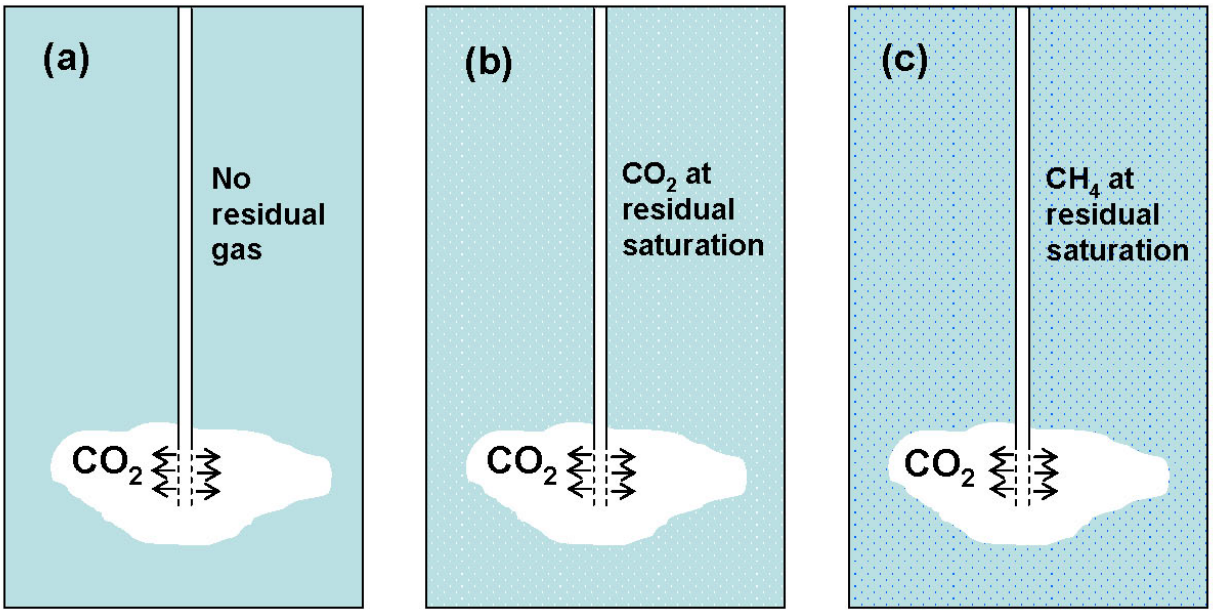

Figure 1. Three alternative cases for injection of CO_2. (a) zero residual gas. (b) 20% residual gas consisting of CO_2 (white stipple). (c) 20% residual gas consisting of CH_4 (dark stipple).

The factors that make this problem potentially interesting are illustrated in Figures 2 and 3. Figure 2 shows a plot of density and viscosity for gas-mixture compositions between pure CO_2 and pure CH_4 as a function of pressure at reservoir temperatures of 40 ^{o}C (left-hand side) and 90 ^{o}C (right-hand side). Density in the figures is calculated using WebGasEOS (Reagan and Oldenburg, 2006), a publicly available web-based tool for calculating gas-mixture properties, which implements the Peng-Robinson equation of state for density, and the method of Chung et al. (1988) for viscosity. As shown, the properties of the mixture vary strongly with composition at all pressures and particularly at pressures above the critical pressure of CO_2 (7.4 MPa). The reason for this is that pure CO_2 compresses readily into its supercritical form, but this compressibility is significantly diminished by admixed components such as CH_4, creating the strong compositional dependence on density. One can imagine a scenario in which injected supercritical CO_2 encounters residual CH_4 resulting in a drastic expansion of the gas mixture.

Figures 3a and 3b show typical non-hysteretic curves (van Genuchten (1980) for capillary pressure and liquid relative permeability, and Corey (1954) for gas relative permeability (see Table 1)). As shown, gas relative permeability increases with gas saturation (liquid saturation decreasing), while water relative permeability decreases with increasing gas saturation. The presence of residual gas thus causes the liquid relative permeability to be lower, all other things being equal. Because the injection of large quantities of CO_2 for GCS requires both the injected CO_2 and the native aqueous fluids (brine) to move, the permeability of the formation to both the injected gas and the brine influences injection pressure, along with the size and character of the injected CO_2 plume. Figures 3c and 3d show hysteretic curves using parameters in Table 1, for several possible turning points (i.e., the saturation at which flow process changes from drainage to imbibition or vice versa). As shown, drainage and imbibition branches are distinct from one another, a feature that models the

dependence of capillary pressure and relative permeability on the flow process (drainage or imbibition) that is occurring as well as on the saturation history (Doughty, 2007). Moreover, imbibition branches with different turning points have different values of residual gas saturation S_{gr}. In Figures 3c and 3d, the drainage branches (red) and the imbibition branches with turning points at S_{lr} (blue) form an envelope in which other imbibition branches lie. Values of S_{gr} range from 0 for the drainage branch to $S_{grmax} = 0.2$ for the imbibition branch with turning point at S_{lr}.

Prior to injection of CO_2 into depleted gas reservoirs, we envision a history of imbibition during the gas-production phase, i.e., as gas is produced, water flows into the formerly gas-filled regions of the reservoir, entrapping residual gas. By this argument, our simulations of CO_2 injection into the water leg of a depleted reservoir should begin on the imbibition branch of the hysteretic curves with turning point S_{lr}. However, the injection of the gas (CO_2) itself is a drainage process. In short, the part of the domain near the well experiencing CO_2 injection (gas saturation increasing) has capillary pressure defined by the second-order drainage branch of the capillary pressure curve (Figure 3c), while the region where brine is being displaced with unchanged gas saturation remains on the imbibition branch.

Our hysteretic formulation (Doughty, 2009) for relative permeability does not distinguish between first-order imbibition and second-order drainage, as indicated by the two-way arrows on Figure 3d. This approximation has worked well for previous problems involving CO_2 injection into saline formations. However, for the present problem, this approximation will not adequately represent the second-order drainage accompanying injection of CO_2 into residual gas. Therefore, being guided by the form of the capillary pressure curve, in which the second-order drainage branch rapidly approaches the primary drainage branch as S_g increases (green dashed line in Figure 3c), for relative permeability we approximate the second-order drainage branch by the first-order imbibition branch with turning point at $S_l = 0.6$ (green dashed line in Figure 3d), but use a slightly increased value of $S_{grmax} = 0.265$, which makes $S_{gr} = 0.2$ and assures that the initial conditions represent immobile gas. Although admittedly ad hoc, this approach captures the essential features of the problem: it preserves the zero gas relative permeability far from the injection well while enabling a rapidly-increasing gas relative permeability near the injection well. Of course, it would be preferable to incorporate the second-order drainage branches directly in the relative permeability functions, and such an effort is planned as part of continuing code development.

This study is aimed at understanding the role of residual gas, from both the phase-interference and compositional perspectives, in controlling CO_2 injection processes. Fluid flow problems in which drainage and imbibition occur in different regions at different times cannot be fully captured using non-hysteretic curves, but it is of interest to see if any relevant features of the problem can be represented using the simpler non-hysteretic forms.

(a)

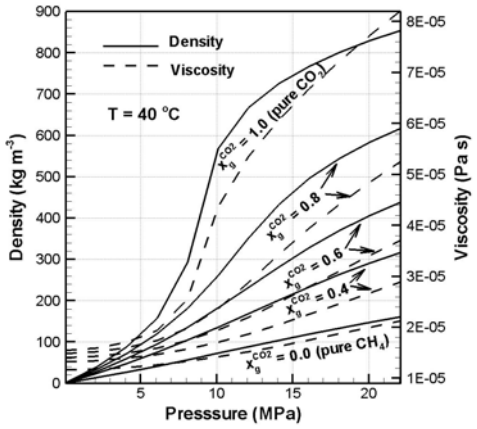

(b)

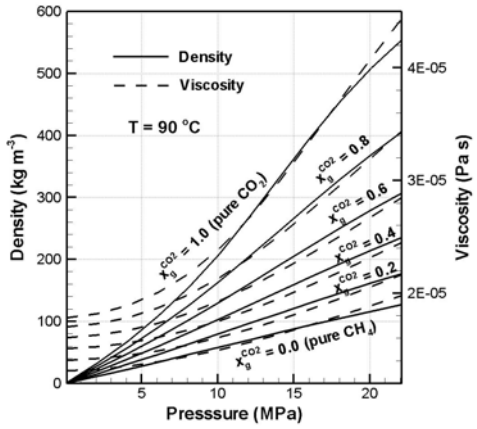

Figure 2. Variation of gas density and viscosity as a function of CO_2-CH_4 mole fraction and pressure at (a) 40 ^oC and (b) 90 ^oC.

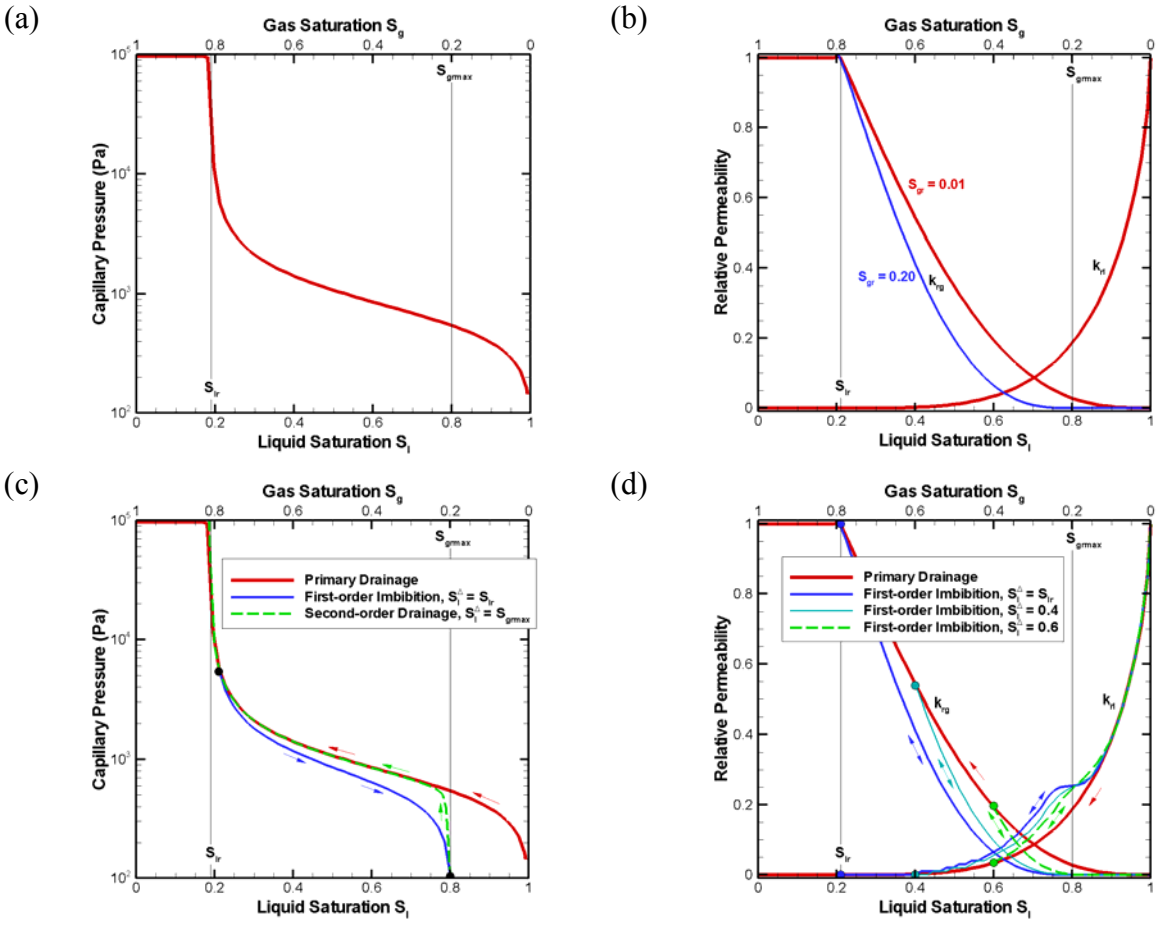

Figure 3. Non-hysteretic variation of (a) capillary pressure and (b) gas and liquid relative permeability as a function of liquid saturation using functions given in Table 1 and two different S_{gr} values. Hysteretic variation of (c) capillary pressure and (d) gas and liquid relative permeability using functions given in Table 1, for several possible turning points (dots). The drainage branches (red) and the imbibition branches with turning points at S_{lr} (blue) form an envelope in which other imbibition branches lie. Arrows identify whether drainage (S_g increasing) or imbibition (S_l increasing) occurs on a given branch.

Methods

Injection simulations were carried out using TOUGH2/EOS7C (Pruess et al., 1999; Oldenburg et al., 2004) to accurately model multiphase flow and multicomponent CO_2 and CH_4 gas-mixture properties. TOUGH2/EOS7C models five components (water, brine, CO_2, a tracer, and CH_4). TOUGH2/EOS7C uses the Peng-Robinson equation of state to calculate gas-mixture density, and the method of Chung et al. (1988) for calculating mixture viscosity. EOS7C uses a fugacity equilibrium approach for gas-mixture solubility that is well-suited for deep reservoir environments (Oldenburg et al., 2004). Salinity effects on gas solubility in the aqueous phase are not modeled, and we have used pure water (zero salinity) as the aqueous phase in the results shown below. To investigate the phase

interference effects of the presence of residual gas on injection in a simplified geometry, we have used both hysteretic and non-hysteretic models as implemented in iTOUGH2/EOS7C (Finsterle, 2004, 2008; Doughty, 2007, 2009).

For this problem, a one-dimensional radial grid was used to emphasize the residual-gas effects being investigated without the complications added by a more complicated geometry. The discretization of the one-dimensional radial problem is shown in Figure 4, emphasizing the details of the fine discretization around the well. Beyond the near-well region, grid spacing is uniform (2 m) out to a radial distance of 300 m (the maximum extent of CO_2 during the 2-year simulation period), beyond which the grid gradually coarsens. Preliminary studies using a grid that gradually coarsened over all r showed that fronts can be significantly smeared out by numerical dispersion. The constant-pressure boundary condition at r = 1074 m was chosen to model the presence of a gas cap somewhere in the system that would tend to moderate pressure changes during water-leg CO_2 injection. The injection rate is 100 t CO_2/day (1.16 kg/s) into a 30-m thick layer with permeability of 500 mD (5×10^{-13} m^2) and porosity equal to 0.20. Two different reservoir scenarios are considered: (1) a 1 km-deep reservoir with initial pressure $P = 1 \times 10^7$ Pa, $T = 40$ °C; and (2) a 2 km-deep system with initial pressure $P = 2 \times 10^7$ Pa, $T = 90$ °C. All simulations are isothermal. The residual gas saturation S_{gr} is set to 0.20 or 0.01 for the non-hysteretic case, to mimic various aspects of the hysteretic case, in which $S_{gr} = 0$ during drainage and S_{gr} varies from 0 to $S_{grmax} = 0.2$ during imbibition. See Table 1 for specific values of parameters, and Figure 3 for the capillary pressure and relative permeability curves used in the simulations. Note that a small amount of CH_4 is co-injected in all the simulations for an efficient numerical solution, but it does not materially affect the results.

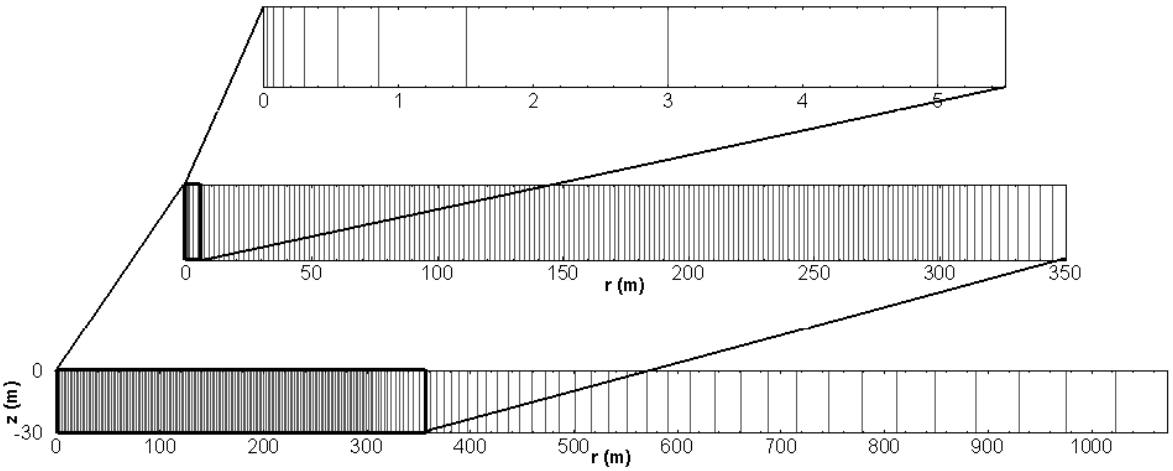

Figure 4. Discretization of the one-dimensional radial problem showing detail around the well at r = 0 m. All boundaries are closed except the right-hand side which is held at constant pressure.

Table 1. Properties of the idealized one-dimensional radial model reservoir.

Thickness	30 m
Radius	1 km (open right-hand side boundary, see Fig. 4)
Porosity (ϕ)	0.2
Pressure (Pa)	Shallow reservoir case: 1 x 10^7 Pa Deep reservoir case: 2 x 10^7 Pa
Temperature (T)	Shallow reservoir case: 40 ^{o}C Deep reservoir case: 90 ^{o}C
Permeability (k)	5 x 10^{-13} m^2
Capillary Pressure (P_c)	van Genuchten[1,2] λ = 0.63, S_{lr} = 0.19, α = 1.5 x 10^{-3} Pa^{-1}, P_{max} = 1 x 10^5 Pa, S_{ls} = 1.
Relative permeability (k_r)	Non-hysteretic liquid: van Genuchten[1,2]; Gas: Corey[3] λ = 0.63, S_{lr} = 0.21, S_{gr} = 0.20 or 0.01 Hysteretic liquid and gas relative permeability[4] λ = 0.63, S_{lr} = 0.21, S_{grmax} = 0.20, γ = 2, λ_{gas} = 0.5
Molec. diffusivity coefficients (d_β^κ)[1]	Liquid: 10^{-10} m^2 s^{-1} Gas: 10^{-5} m^2 s^{-1} θ = 0.0, P_0 = 10^5 Pa
Tortuosity (τ_0)	0.25
Saturation-dependent tortuosity (τ_β)	Equal to relative permeability

[1]Pruess et al. (1999)
[2]λ is m in van Genuchten (1980)
[3]Corey (1954)
[4]Doughty (2007, 2009)

Results

Pressure (P), liquid saturation (S_l), mass fraction of CO_2 in the gas (X_g^{CO2}), gas density (ρ_g), and mass fraction of CH_4 in the gas (X_g^{CH4}) for the three cases considered are shown in Figures 5–7 for a shallow reservoir (P = 1 x 10^7 Pa, T = 40 ^{o}C) and for a deep reservoir (P = 2 x 10^7 Pa, T = 90 ^{o}C). Results from both hysteretic and non-hysteretic relative permeability curves (with two different values of residual gas saturation) are presented for P and S_l, the differences between which will be discussed first for each of the three cases.

In particular, for the case of no residual gas (Figure 5) the pressure curves reveal differences for hysteretic and non-hysteretic results. Pressure rise for the case of non-hysteretic S_{gr} = 0.20 is larger than for the cases of non-hysteretic S_{gr} = 0.01 and hysteretic relative permeability. The reason for the difference is that non-hysteretic S_{gr} = 0.20 requires the gas saturation in the injection zone to exceed 0.20 before CO_2 becomes mobile, hence the pressure builds up more before flow occurs. For non-hysteretic S_{gr} = 0.01, CO_2 with gas saturation exceeding 0.01 is mobile, thus creating less

pressure build up. The hysteretic case involves gas relative permeability following the drainage branch as CO_2 is injected, which matches closely the non-hysteretic $S_{gr} = 0.01$ case. For locations beyond the gas front, pressures are nearly equal for non-hysteretic and hysteretic cases because there is no gas saturation to cause phase interference. Note in this first scenario the CO_2 plume extends to r = 140 m after two years.

Figures 6 and 7 show results for the cases of CO_2 injection into the system with gas at residual saturation. The results for pressure show large differences between hysteretic and non-hysteretic curves and for the two different values of S_{gr}. The small pressure increase obtained for non-hysteretic curves with $S_{gr} = 0.01$ arises because gas is mobile at nearly all saturations. In contrast, for $S_{gr} = 0.20$, the gas relative permeability near the well and the liquid relative permeability beyond the injected gas plume are lower than in the $S_{gr} = 0.01$ case causing greater pressure increase. The hysteretic pressure profile is intermediate between these extremes as it models drainage conditions near the well and imbibition conditions beyond the injected plume front. The hysteretic liquid saturation profile is also intermediate between the non-hysteretic profiles over most of the plume. At low liquid saturations (small r), the hysteretic profile follows the non-hysteretic profile with S_{gr} = 0.01. Starting at $S_l = 0.6$ it then parallels the non-hysteretic profile with $S_{gr} = 0.20$. This behavior reflects the gas-phase relative permeability curve shown in Figure 3d, in which the dashed line used to represent the second-order drainage branch coincides with the primary drainage branch for $S_l \leq$ 0.6, but more closely resembles the first-order imbibition branch for $S_l > 0.6$. Comparing Figure 3d to Figure 3b indicates that the primary drainage and first-order imbibition branches are identical to the non-hysteretic gas relative permeability curves for $S_{gr} = 0.01$ and $S_{gr} = 0.20$, respectively.

Considering now just the hysteretic results of Figures 5 and 6, we see the first-order observation that the pressure increase at the well is larger for the case with residual CO_2 gas (Figure 6) than for the case of fully saturated conditions with zero residual gas (Figure 5). This occurs because of the decreased mobility of brine in the cases where residual gas is present. By this mechanism, rather than enhancing injectivity as might be expected by the presence of gas at the outset, residual gas inhibits injectivity by limiting the mobility of the brine that must be displaced in order for injection to occur. The second observation from comparison of results of Figures 5 and 6 is that the plume radius as defined by the region in which gas is mobile is larger in Figure 6 than in Figure 5. Specifically, in the case of zero residual gas (Figure 5), the injected CO_2 plume extends approximately 140 m as defined by the gas saturation. For the case with residual CO_2 gas (Figures 6), the gas saturation front extends about 230 m. Apparently, the injected gas is augmented by the initial residual gas which is incorporated into the mobile gas plume. Some of this increase in plume extent occurs because a small fraction of the injected CO_2 dissolves when no CO_2 is initially present. Without this dissolution, simulation results (not shown) indicate that the plume in the no-residual-gas case would extend to about 160 m.

We now consider the most interesting case, that of supercritical CO_2 injection into a system with residual CH_4 gas. Comparing only the hysteretic results, we observe the pressure rise is slightly lower for the case of supercritical CO_2 injection into the system with residual CH_4 (Figure 7) than into the system with residual CO_2 (Figure 6). The reason for this appears to be the lower viscosity of CH_4 gas relative to supercritical CO_2. Apparently the displacement of CH_4 ahead of the CO_2 injection front requires less pressure than does the displacement of CO_2. The drastic reduction in gas-mixture density as supercritical CO_2 mixes with CH_4 reveals itself as a third-order effect in the

liquid saturation curve which shows the larger gas plume size (r = 260 m for the shallow reservoir and r = 240 m for the deep reservoir) (Figure 7) relative to the gas plume size (r = 230 m) in Figure 6. The effect is stronger for the lower pressure and temperature case than for the higher pressure and temperature case. This large decrease in density causes a volume expansion that is also reflected in the shape of the liquid saturation curve. In contrast to the smooth increase in liquid saturation with radial distance shown in Figure 6, the liquid saturation curve in Figure 7 shows two distinct regions: one from r = 0 to r = 140 m (where gas is predominantly CO_2) and the other from r = 140 m to r = 260 m (where gas is predominantly CH_4) with a notable break in slope at the transition from CO_2 to CH_4. Note as an aside that the local maximum in liquid saturation (minimum in gas saturation) near the plume front for the non-hysteretic case (S_{gr} = 0.01) is an artifact of the non-hysteretic relative permeability model and does not occur for the hysteretic case. In short, the simulations show that supercritical CO_2 mixes with residual CH_4 causing the total volume of gas to increase, which creates a larger gas plume relative to the residual-CO_2 gas case.

For the conditions considered here, the radial extent of the plume increases by almost a factor of two when residual CH_4 is present (260 m, Figure 7) compared to injection into a formation with no residual gas (140 m, Figure 5). This finding raises the question of how much, if at all, plume extent would increase for CO_2 injection into a liquid-saturated formation containing dissolved CH_4, which is considered a likely scenario for CO_2 injection into the water leg of a depleted gas reservoir or a saline formation located in the vicinity of a petroleum resource. Figure 8 shows simulation results for a case in which the formation initially contains dissolved CH_4 just below the solubility limit. Comparison of the saturation profiles for Figures 5 and 8 shows that they are identical right up to the leading edge, where the plume for the dissolved CH_4 case extends about 10 m farther, to r = 150 m. The mass fraction profile indicates that the plume is nearly pure CO_2 out to r = 140, then nearly pure CH_4 at the leading edge, indicating that as CO_2 moves out into the formation, creating a gas phase and partially dissolving into the liquid phase, the initially-dissolved CH_4 exsolves immediately, and is then pushed ahead of the growing CO_2 plume. Because the mass of CH_4 initially present for the dissolved case (Figure 8) is much smaller than for the residual gas case (Figure 7), the increase in radial extent of the plume is correspondingly much smaller.

In summary, the three main effects observed in the preceding simulations are (1) the reduction in injectivity caused by decreased brine mobility due to the presence of residual gas regardless of composition, (2) the larger extent of the gas plume caused by incorporation of dissolved or residual gas into the injected gas plume, and (3) the expansion of the gas plume caused by mixing of injected CO_2 with residual CH_4. Hysteretic relative permeability is needed to model properly all of the variables over the whole domain, although non-hysteretic models can be used for modeling parts of the system.

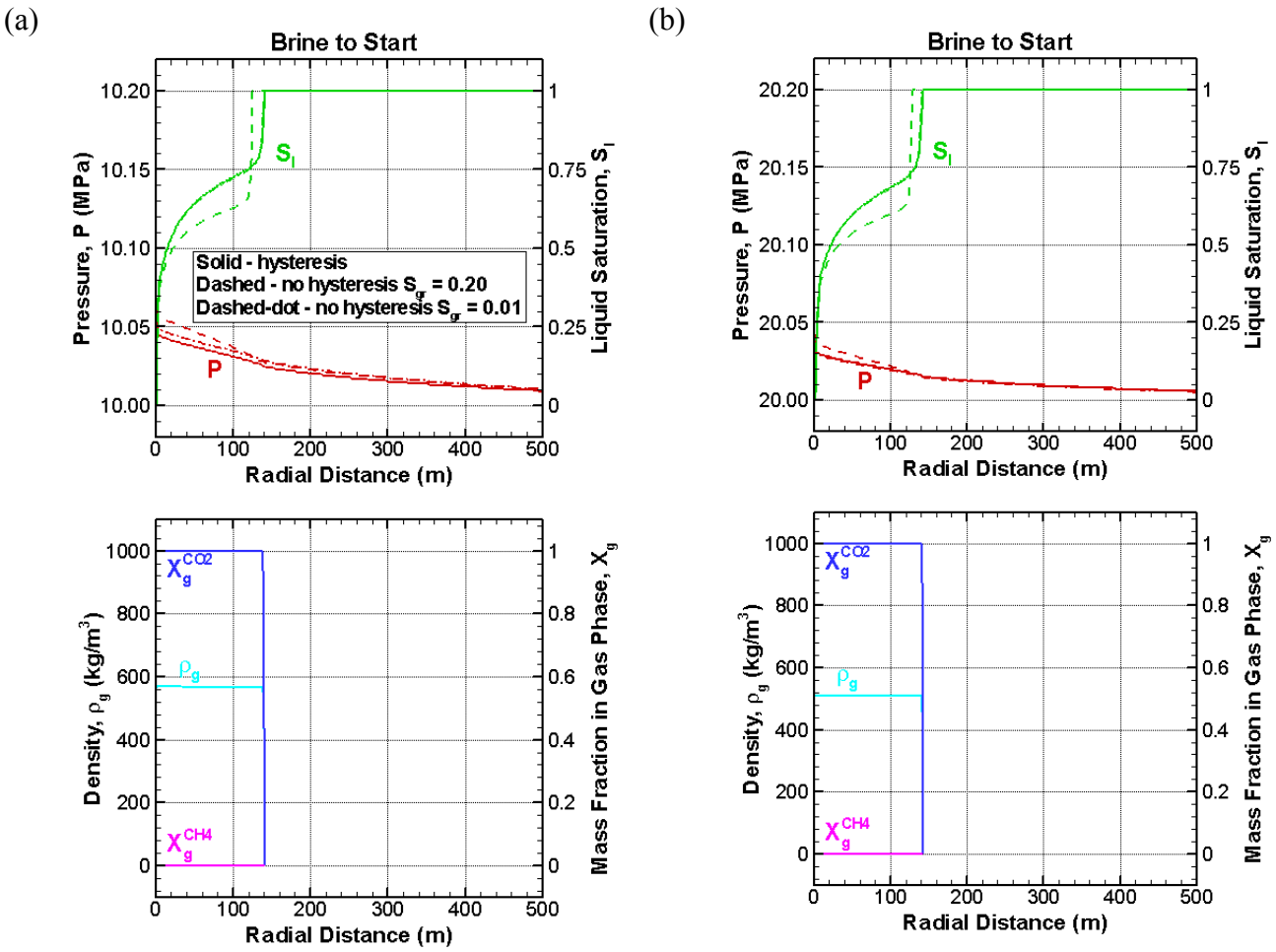

Figure 5. Results after two years of injection of CO_2 into a formation saturated with brine, showing pressure, saturation, gas density (kg m^{-3}), and mass fractions for the shallow (a) and deep (b) reservoirs. In the upper frames, where the dash-dot line is not visible, it coincides with the solid line.

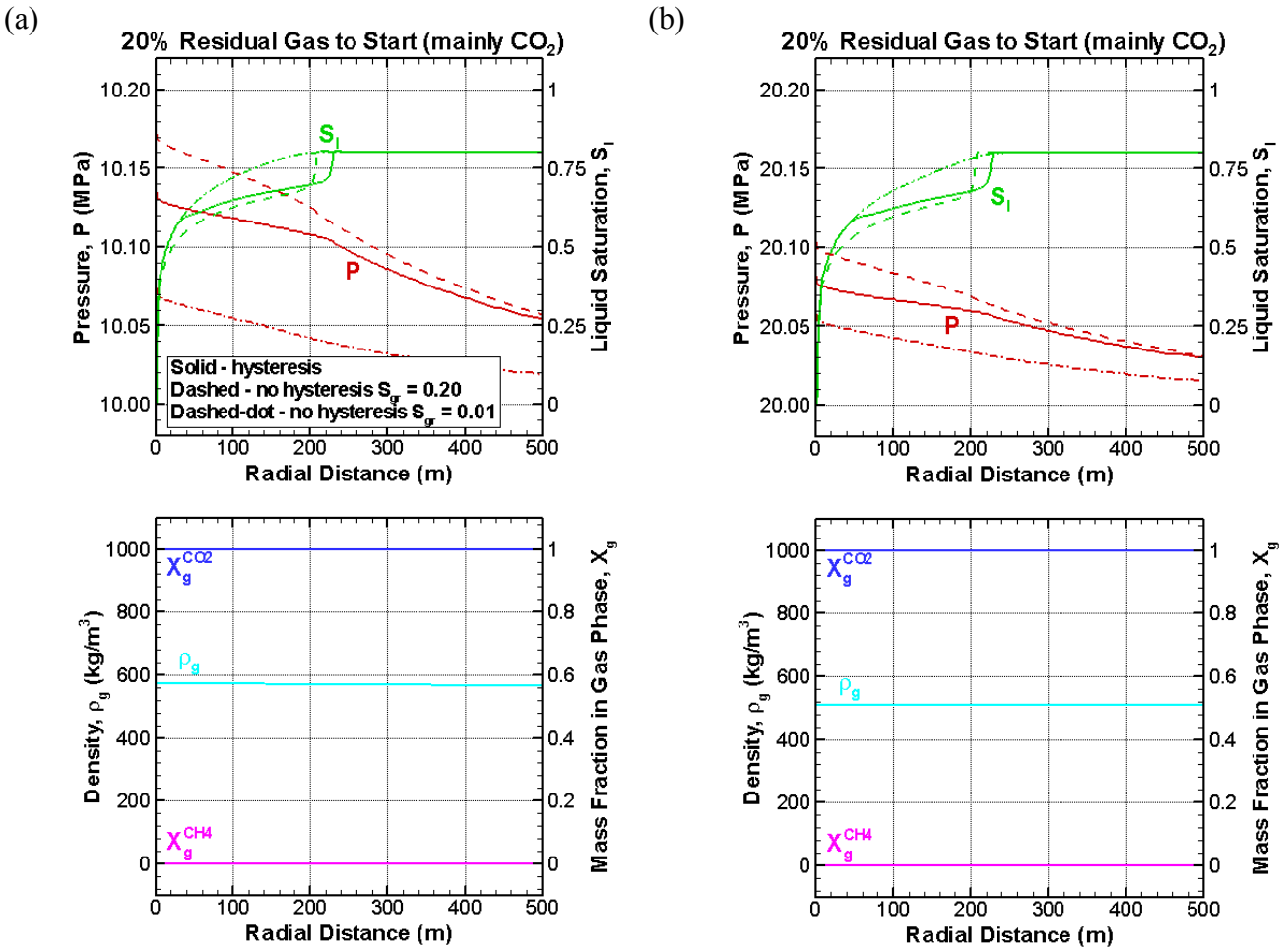

Figure 6. Results after two years of injection of CO_2 into a formation containing 20% residual gas consisting mainly of CO_2, showing pressure, saturation, gas density (kg m^{-3}), and mass fractions for the shallow (a) and deep (b) reservoirs.

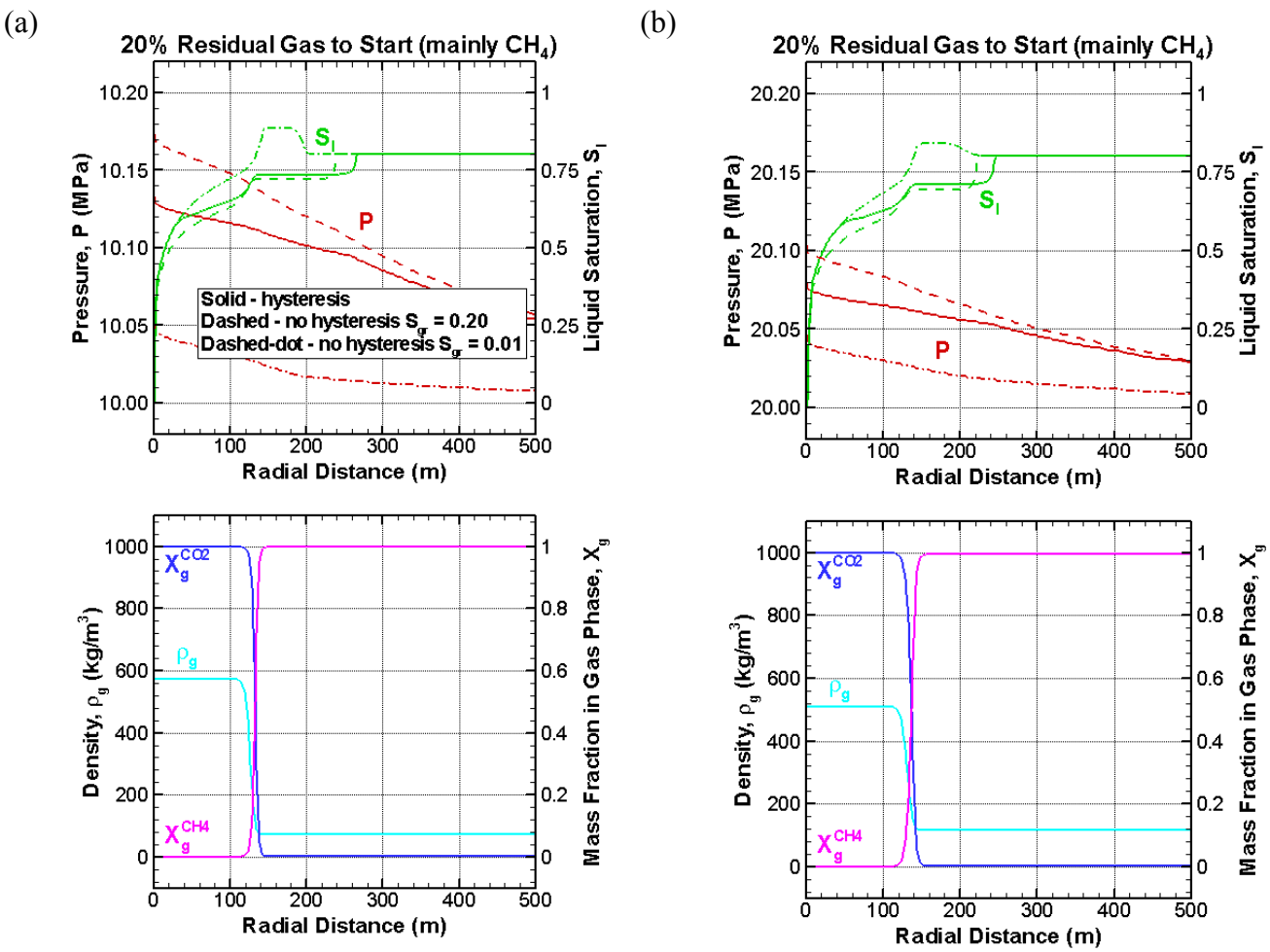

Figure 7. Results after two years of injection of CO_2 into a formation containing 20% residual gas consisting mainly of CH_4, showing pressure, saturation, gas density (kg m^{-3}), and mass fractions for the shallow (a) and deep (b) reservoirs.

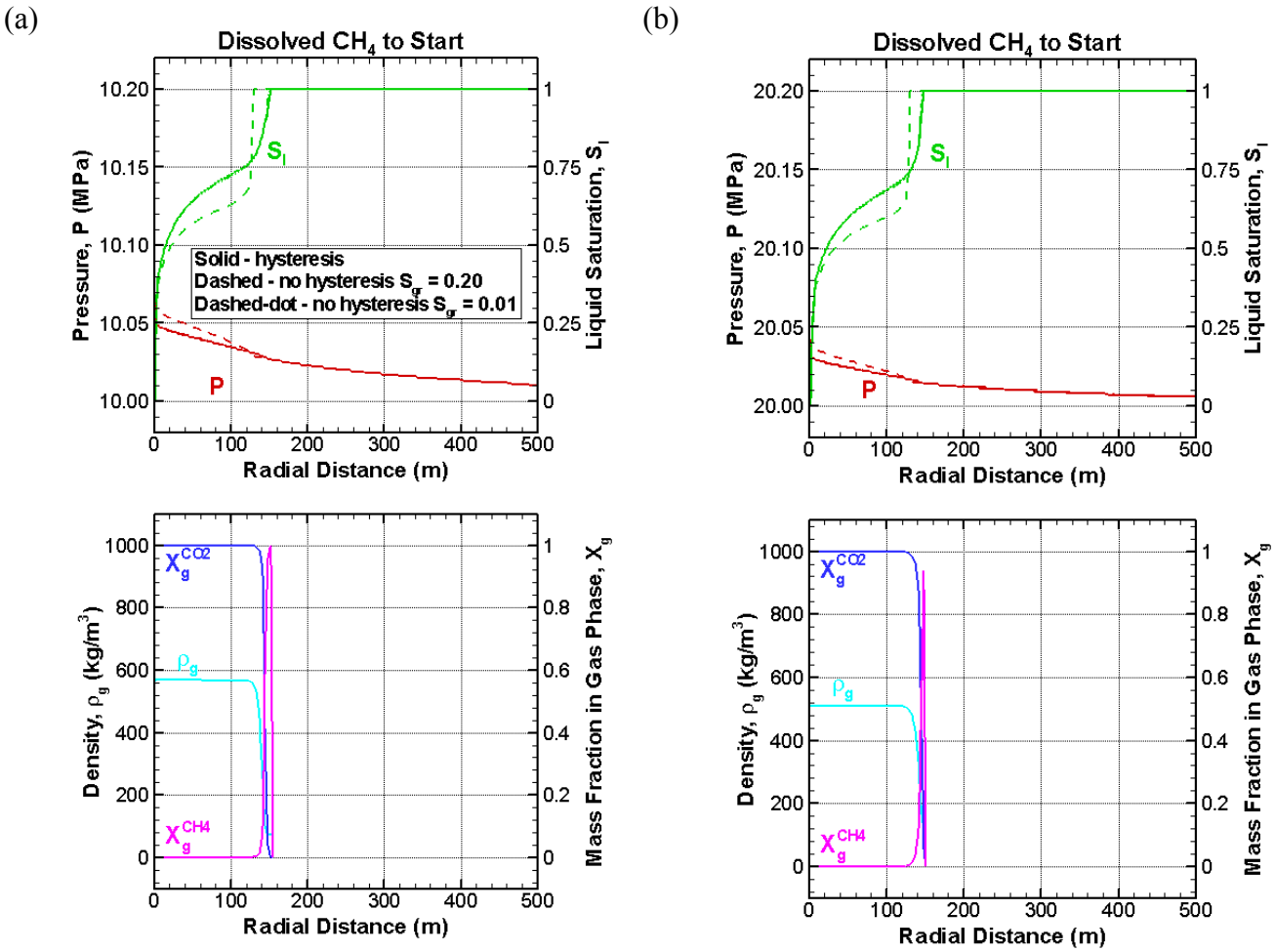

Figure 8. Results after two years of injection of CO_2 into a formation containing dissolved CH_4 just below the solubility limit, showing pressure, saturation, gas density (kg m^{-3}), and mass fractions for the shallow (a) and deep (b) reservoirs. In the upper frames, where the dash-dot line is not visible, it coincides with the solid line.

Effects of Alternative Outer Radial Boundary Conditions

To examine the impact of the constant-pressure boundary approximately 1 km from the injection well, several cases with an infinite-acting reservoir were also modeled. For these cases, the grid extends 100 km, farther than any of the pressure responses propagate during the two-year injection period. Figure 9a shows results for a shallow formation containing dissolved CH_4 (compare to Figure 8a) and Figure 9b shows results for a shallow formation containing 20% residual CH_4 gas (compare to Figure 7a). The only noticeable differences are the pressure profiles, which are about 0.05 MPa higher for the infinite-acting reservoir. The resulting density increase is barely noticeable (as expected based on Figure 2a), and the saturation and mass fraction profiles are essentially unchanged. Simulation results for other initial conditions are comparable. Thus we can conclude that as far as plume development goes, the open reservoir model is equivalent to an infinite reservoir model.

A more extreme change in the outer radial boundary condition is to consider a closed reservoir. This is easily modeled by replacing the constant-pressure grid block at r = 1074 m in the original grid (Figure 4) with a normal grid block. Figure 10 shows results for a closed shallow reservoir after two years for the cases with dissolved CH_4 initially present (Figure 10a; compare to Figures 8a and 9a) and 20% residual CH_4 initially present (Figure 10b; compare to Figures 7a and 9b). For the closed right-hand side boundary condition, there is a large pressure increase accompanying CO_2 injection when no gas is initially present (Figure 10a) because liquid compressibility is small, enabling the pressure response to propagate rapidly to the closed boundary. The large pressure increase (about 7.6 MPa, compared to less than 0.1 MPa for the open and infinite-acting cases) causes CO_2 density to increase dramatically (from 570 kg/m^3 to 795 kg/m^3), resulting in a more compact CO_2 plume (a plume extent of r =120 m at two years rather than the r = 150 m previously obtained). In contrast, when residual gas is initially present, fluid compressibility is significantly larger, and the closed boundary has only a small effect (Figure 10b), with pressure increasing about 0.15 MPa more than for the open case and 0.10 MPa more than for the infinite-acting case. This completely closed reservoir is probably not a realistic choice for actual CO_2 storage, but it serves as a limiting case for the more promising "semi-closed" reservoirs, which are bounded radially, but allow significant pressure release through under- and overlying shale layers (Zhou et al., 2009).

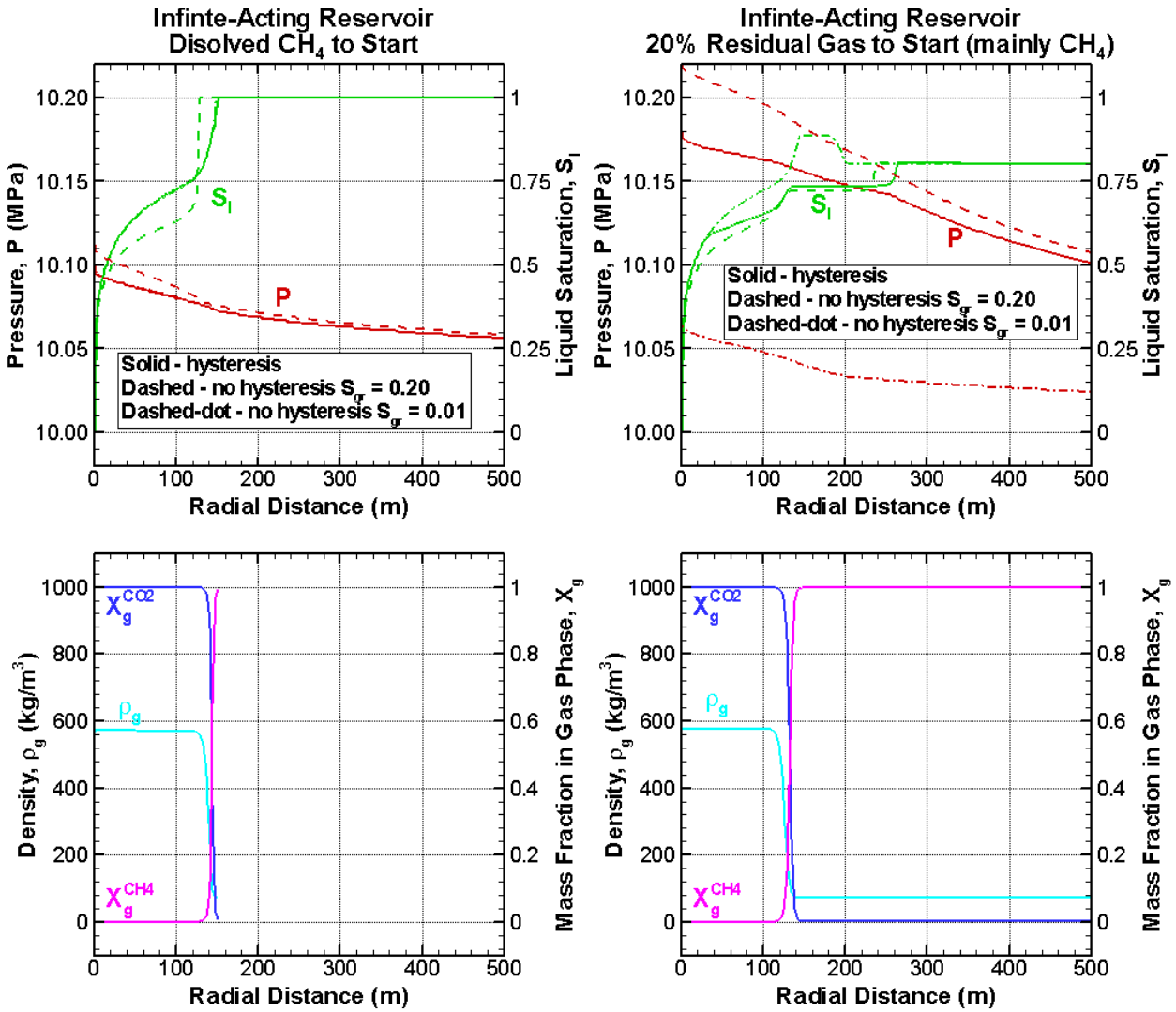

Figure 9. Results after two years of injection of CO_2 into an infinite-acting shallow reservoir containing (a) dissolved CH_4 and (b) 20% residual gas consisting mainly of CH_4, showing pressure, saturation, gas density (kg m^{-3}), and mass fractions. In the upper frames, where the dash-dot line is not visible, it coincides with the solid line.

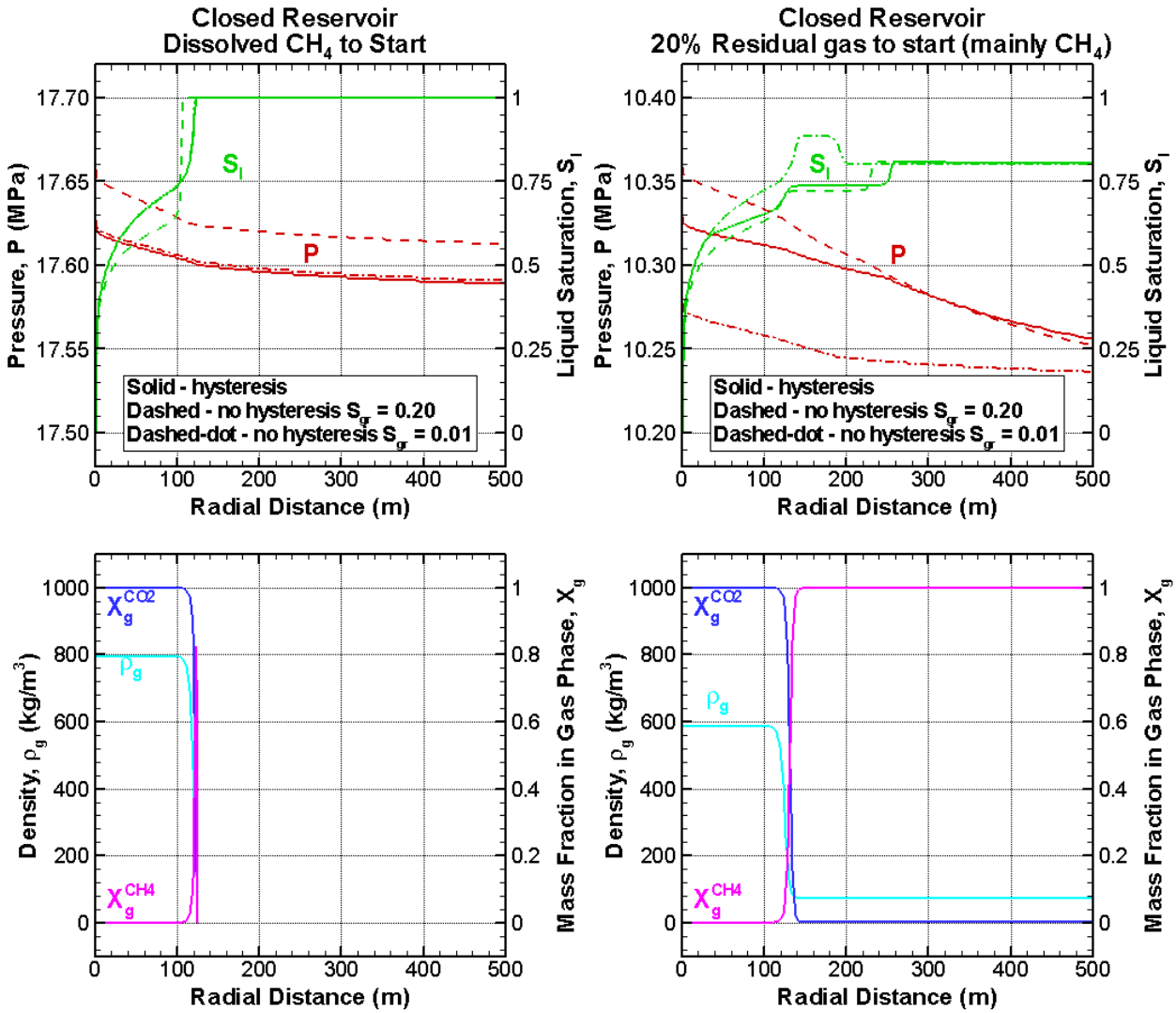

Figure 10. Results after two years of injection of CO_2 into a closed shallow reservoir containing (a) dissolved CH_4 and (b) 20% residual gas consisting mainly of CH_4, showing pressure, saturation, gas density (kg m^{-3}), and mass fractions. In the upper frames, where the dash-dot line is not visible, it coincides with the solid line. Note the two different pressure scales for (a) and (b); initial reservoir pressure is 10 MPa for both.

Displaying Results as Transients for Observation Well Locations

Displaying simulation results as a function of radial distance for a given time provides an excellent way to visualize the multi-phase flow and transport processes accompanying CO_2 injection, but it is not necessarily the optimal approach for designing field experiments or interpreting field data. Rather than having a complete picture of pressure, saturation, and gas content throughout the subsurface at a given time, we typically have a transient record from a limited number of observation wells. Figure 11 shows the simulation results for four years of CO_2 injection into open and closed shallow reservoirs for initial conditions of brine nearly saturated with dissolved CH_4, as the transient response at three observation wells located 50, 100, and 150 m away from the injection well. Figure 12 shows the same results for initial conditions of brine containing 20% residual CH_4.

The open-reservoir case satisfies the conditions required for a similarity-variable r^2/t to exist: one-dimensional radial geometry, essentially infinite radial extent, spatially uniform material properties and initial conditions, and steady flow rate at the injection well. Thus, the transient responses at each observation well can be collapsed to a single curve by dividing each time by the r^2 value of that well. Such an exercise can provide useful insight into grid discretization errors, and in fact was used for that purpose here, to confirm that the 2-m grid spacing within the domain of the CO_2 plume is adequate. However, plotting versus t/r^2 does not illustrate the actual timing of CH_4 and CO_2 arrival as well as plotting versus t does. For example, Figure 11a illustrates clearly that as observation well distance increases, the duration of the CH_4 pulse at the leading edge of the CO_2 plume increases.

The difference in pressure response for the open and closed reservoirs is strikingly displayed in the transient plots. When plotted on a scale big enough to show the entire range of pressures reached for the closed reservoir, as is done in Figure 11, the responses for the different observation wells collapse to a single curve. That is, the pressure over the entire model is roughly uniform. For the open reservoir (Figure 11a), this uniform pressure is essentially constant, so the gas density is purely a function of gas-phase composition. In contrast, for the closed reservoir (Figure 11b), as pressure increases, CO_2 density increases sharply and CH_4 density increases modestly (consistent with Figure 2a), and this variation is superposed on the gas-phase composition dependence as CH_4 and CO_2 arrive at each observation well. The overall density increase makes the plume much more compact, greatly lengthening the arrival time at more distant observation wells.

When residual gas is present (Figure 12), the difference between open and closed reservoir cases is much smaller, as the overall pressure increase for the closed reservoir case is small. Here the transient response highlights how long a time delay there is between the arrival of the plume (as manifested by a liquid saturation decrease) and the arrival of CO_2 at an observation well, and how this delay grows significantly as observation well distance from the injection well increases. In contrast to the dissolved CH_4 initial condition, where the CH_4 pulse is rather narrow (Figure 11), when residual CH_4 is initially present, CO_2 arrival may not occur for a considerable time after the initial decrease in S_l (Figure 12). For example, for the 100-m observation well, with dissolved CH_4 initially present, CO_2 begins to arrive simultaneously with the initial S_l decline, whereas with residual CH_4 initially present, there is a delay of more than 200 days between initial S_l decline and CO_2 arrival.

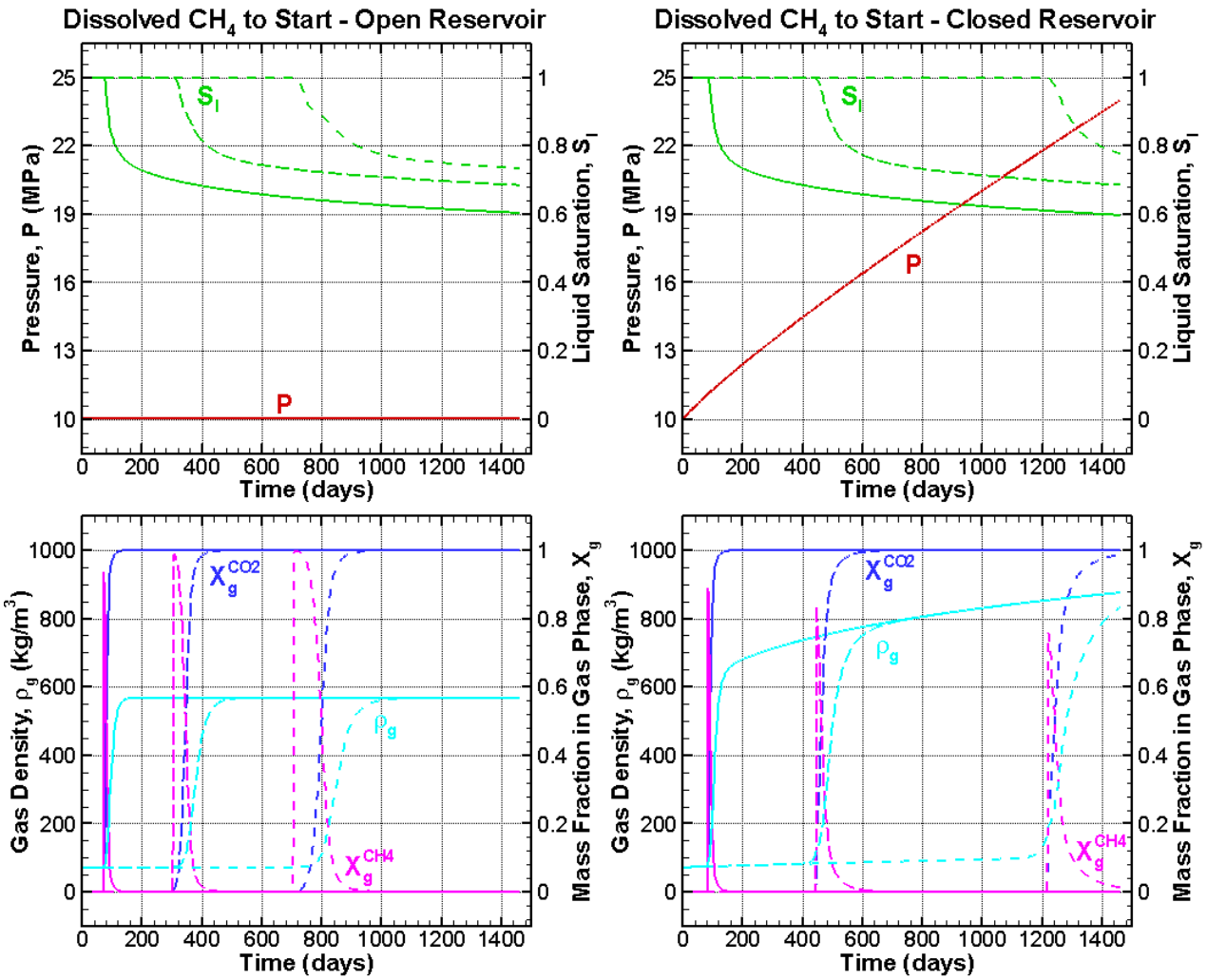

Figure 11. Transient response at 50 m (solid), 100 m (long dash), and 150 m (short dash) away from the injection well for CO_2 injection into (a) open and (b) closed shallow reservoirs containing brine with dissolved CH_4. When no gas phase exists ($S_l = 1$), gas mass fractions are shown as zero and ρ_g shows the density a gas phase would have if it were present.

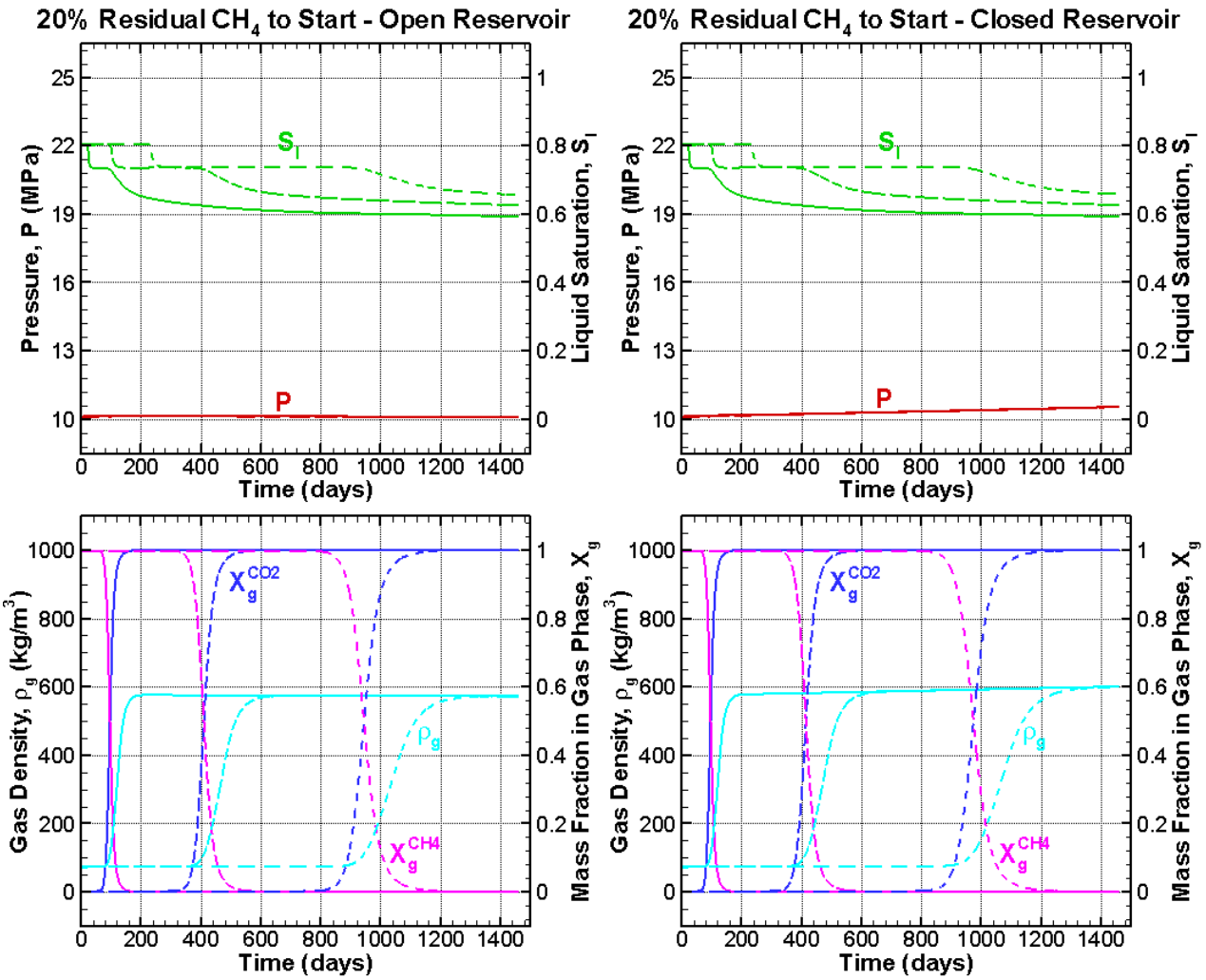

Figure 12. Transient response at 50 m (solid), 100 m (long dash), and 150 m (short dash) away from the injection well for CO_2 injection into (a) open and (b) closed shallow reservoirs containing brine with 20% residual CH_4.

Figure 13 summarizes all the effects of initial and boundary conditions on plume development by plotting plume arrival time at each observation well for all cases modeled. For an open or infinite-acting reservoir, the arrival time of the plume at a given observation well decreases sharply as one goes from a brine-saturated formation, to a formation containing dissolved gas, to a formation containing residual gas. For example, for an observation well located 100 m from the injection well, the plume would be expected 372 days after injection commenced for a brine-saturated formation, at 303 days for a formation with dissolved CH_4, and at 98 days for a formation with residual CH_4. For a closed reservoir, arrival times for cases with no residual gas initially present are significantly longer, due to the density increase accompanying pressure increase. The effect of the composition of the gas initially present is relatively small. For dissolved gas, arrival time is slightly earlier when CO_2 is initially present because none of the injected CO_2 can dissolve (when CH_4 is initially present, some CO_2 dissolves into the aqueous phase and some CH_4 exsolves, but the net effect is more dissolution and a later plume arrival). For residual gas, arrival time is slightly later when CO_2 is initially present, because the greater density of CO_2 results in a more compact plume.

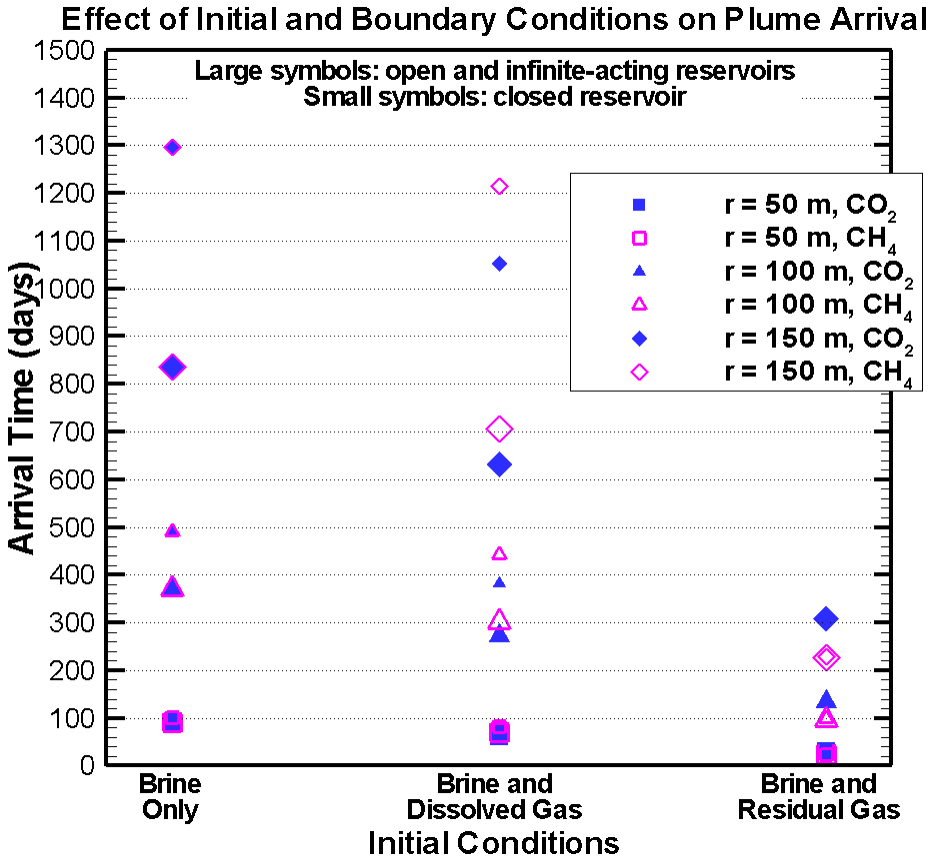

Figure 13. Plume arrival time at observation wells located 50, 100, and 150 m from the injection well, for various initial and boundary conditions. Symbol color identifies the composition of the gas initially present.

Summary, Conclusions, and Future Work

Applications of TOUGH2/EOS7C with and without hysteretic relative permeability were carried out to investigate the effects of residual gas on CO_2 injection in depleted gas reservoirs. Results suggest that residual gas reduces injectivity by reducing the mobility of the brine that has to be displaced. A secondary effect is the tendency for the gas plume to extend farther from the injection well as residual gas is incorporated into the mobile gas plume. The extent is greater when the residual gas is CH_4, with its much lower density than supercritical CO_2, which strongly decreases plume density, resulting in a larger plume volume. When a closed reservoir is considered, pressure can increase significantly during injection, which in turn increases CO_2 density, creating a plume that grows more slowly as time goes on.

The maximum increase in radial extent of the injected gas plume is about a factor of two in the one-dimensional system investigated here, and could be somewhat larger in a two-dimensional (r,z) system where buoyancy flow can be included, since the lower gas density caused by the mobilized CH_4 will make the plume more buoyant. While a factor of two increase in plume extent is certainly non-trivial, it is relatively modest compared to the potential effects of other poorly known system parameters, such as vertical permeability, which controls buoyancy flow and gravity override, and horizontal permeability anisotropy (e.g., due to a contribution from fracture permeability), which controls the direction of plume movement, and other permeability heterogeneity that cause flow channelization.

This preliminary study has motivated future work in several areas. First, using a two-dimensional rz model geometry will enable the interplay of buoyancy flow and initial conditions to be examined, and using a three-dimensional model will allow treatment of dipping formations and incorporation of heterogeneous hydrologic properties, which could promote preferential flow. Second, the impact of varying the capillary pressure and relative permeability parameters should be investigated to address different formation types and associated parameter uncertainty. Laboratory data (e.g., Bachu and Bennion, 2008) suggest that parameters such as residual phase saturations and end-point relative permeability vary over a large range among different rock samples, and this variation is expected to strongly impact both the pressure and saturation responses to CO_2 injection. Finally, a more rigorous treatment of hysteresis is necessary, in which the higher-order scanning curves (2^{nd}-order drainage and 3^{rd}-order imbibition) already incorporated in the capillary pressure function are added to the gas- and liquid-relative permeability formulations.

Acknowledgment

We thank two anonymous reviewers and Dmitriy Silin (LBNL) for constructive comments. This work was carried out with funding from the GEO-SEQ and ZERT projects funded by the Assistant Secretary for Fossil Energy, Office of Sequestration, Hydrogen, and Clean Coal Fuels, through the National Energy Technology Laboratory, U.S. Department of Energy under Contract No. DE-AC02-05CH11231.

REFERENCES

Bachu, S. and B. Bennion, Effects of in-situ conditions on relative permeability characteristics of CO_2-brine systems, *Env. Geology*, 54(8), 1707-1722, 2008.

Blok, K., R.H. Williams, R.E. Katofsky, and C.A. Hendriks, Hydrogen production from natural gas, sequestration of recovered CO2 in depleted gas wells and enhanced natural gas recovery, *Energy*, *22* (2,3), 161–168, 1997.

Chung, T.-H., M. Ajlan, L.L. Lee, and K.E. Starling, Generalized multiparameter correlation for nonpolar and polar fluid transport properties, *Ind. Eng. Chem. Res.*, *27*, 671-679, 1988.

Corey, A.T., The interrelation between gas and oil relative permeabilities, *Producers Monthly*, 38-41, November 1954.

Doughty, C., Modeling geologic storage of carbon dioxide: Comparison of non-hysteretic and hysteretic characteristic curves, *Energy Conv. and Mgmt.*, *48*(6), 1768-1781, 2007.

Doughty, C., User's Guide for Hysteretic Capillary Pressure and Relative Permeability Functions in iTOUGH2, Lawrence Berkeley National Laboratory Report *LBNL-2483E*, August, 2009.

Finsterle, S., Multiphase inverse modeling: Review and iTOUGH2 applications, *Vadose Zone J.*, *3*, 747–762, 2004.

Finsterle, S., C. Doughty, M.B. Kowalsky, G.J. Moridis, L. Pan, T. Xu, Y. Zhang, and K. Pruess, Advanced vadose zone simulation using TOUGH, *Vadose Zone J.*, 7, 601–609, doi:10.2136/vzj2007.0059, 2008.

Koide, H., Y. Tazaki, Y. Noguchi, S. Nakayama, m Iijima, K. Ito, and Y. Shindo, Subterranean containment and long-term storage of carbon dioxide in unused aquifers and in depleted natural gas reservoirs, *Energy Conv. and Mgmt.*, *33*(5-8), 619-626, 1992.

Maloney, D. R., and M. Briceno, Experimental investigation of cooling effects resulting from injecting high pressure liquid or supercritical CO2 into a low pressure gas reservoir, *Petrophysics*, *50*, 335–344, 2009.

Mathias, S.A., J.G. Gluyasa, C.M. Oldenburg and C.-F. Tsang, Analytical solution for Joule–Thomson cooling during CO_2 geo-sequestration in depleted oil and gas reservoirs, *Int. Journal of Greenhouse Gas Control*, doi:10.1016/j.ijggc.2010.05.008, 2010 online.

Oldenburg, C.M., Joule-Thomson cooling due to CO2 injection into natural gas reservoirs, *Energy Conv. and Mgmt.*, *48*, 1808-1815, 2007, LBNL-60158,

Oldenburg, C.M., K. Pruess, and S.M. Benson, Process modeling of CO2 injection into natural gas reservoirs for carbon sequestration and enhanced gas recovery, *Energy&Fuels*, *15*, 293–298, 2001, LBNL-45820.

Oldenburg, C.M., G.J. Moridis, N. Spycher, and K. Pruess, EOS7C version 1.0: TOUGH2 module for carbon dioxide or nitrogen in natural gas (methane) reservoirs, Lawrence Berkeley National Laboratory Report *LBNL-56589*, 2004a. http://repositories.cdlib.org/lbnl/LBNL-273E.

Oldenburg, C.M., S.H. Stevens, and S.M. Benson, Economic feasibility of carbon sequestration with enhanced gas recovery (CSEGR), *Energy*, *29*,1413–1422, 2004b, LBNL-49762.

Pruess, K., C. Oldenburg, and G. Moridis, *TOUGH2 User's Guide, Version 2.0*, Report *LBNL-43134*, Lawrence Berkeley National Laboratory, Berkeley, Calif., 1999.

Reagan, M.T. and C.M. Oldenburg, WebGasEOS v1.0 User Guide, Lawrence Berkeley National Laboratory Report *LBNL-3188*, June 2006.

Ringrose, P., M Atbi, D Mason, M Espinassous, Ø. Myhrer, M. Iding, A. Mathieson and I. Wright, Plume development around well KB-502 at the In Salah CO_2 storage site, *First Break*, *27*, January 2009.

Sharma, S., Cook, P., Berly, T. and Anderson, C., Australia's first geosequestration demonstration project - the CO2CRC Otway Basin Pilot Project. *The APPEA Journal*, 47(1), 257–68, 2007.

van der Burgt, M.J., J. Cantle, and V.K. Boutkan, Carbon dioxide disposal from coal-based IGCCs in depleted gas fields, *Energy Conv. and Mgmt.*, *33* (5–8), 603–610, 1992.

Van der Meer, L.G.H., Hartman, J., Geel, C., Kreft, E., Re-injecting CO2 into an offshore gas reservoir at a depth of nearly 4000 metres sub-sea, GHGT-7, Vancouver, 6-9 September 2004.

van Genuchten, M.Th, A closed-form equation for predicting the hydraulic conductivity of unsaturated soils, *Soil Sci. Soc*., *44*, 892-898, 1980.

Zhou, Q., J. Birkholzer, nd C.-F. Tsang, A semi-analytical solution for large-scale injection-induced pressure perturbation and leakage in a Laterally bounded aquifer–Aquitard system, *Transport in Porous Media*, 78, 127-148, 2009.

DISCLAIMER